(2)

FTD-ID(RS)T-1273-90

AD-A234 798

FOREIGN TECHNOLOGY DIVISION

CHINESE SPACE SCIENCE AND TECHNOLOGY

(Selected Articles)

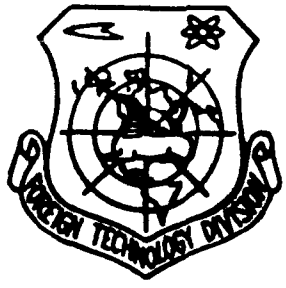

Approved for public release;
Distribution unlimited.

DISCLAIMER NOTICE

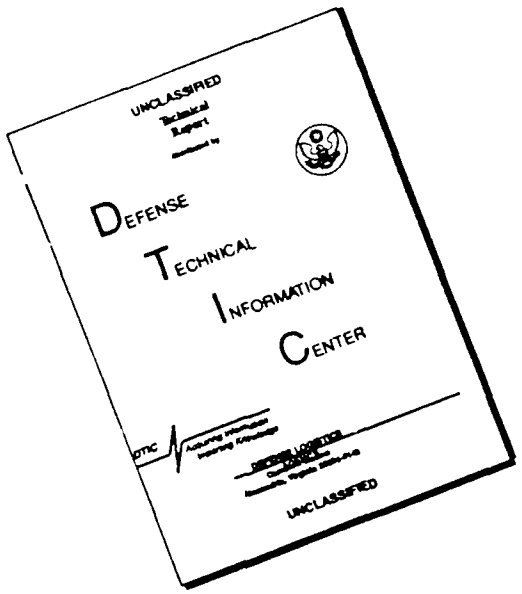

THIS DOCUMENT IS BEST QUALITY AVAILABLE. THE COPY FURNISHED TO DTIC CONTAINED A SIGNIFICANT NUMBER OF PAGES WHICH DO NOT REPRODUCE LEGIBLY.

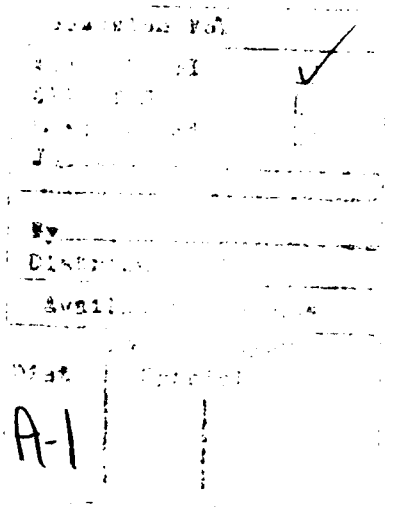

HUMAN TRANSLATION

FTD-ID(RS)T-1273-90 21 March 1991

MICROFICHE NR: FTD-91-C-000244

CHINESE SPACE SCIENCE AND TECHNOLOGY
(Selected Articles)

English pages: 22

Source: Zhongguo Kongjian Kexue Jishu, Vol. 10, Nr. 2, 1990, pp. Title Page; 5-9; 25-29

Country of origin: China
Translated by: SCITRAN
F33657-84-D-0165
Requester: FTD/SDMSS/1Lt Paul A. Lithgow

PREPARED BY:

TRANSLATION DIVISION
FOREIGN TECHNOLOGY DIVISION
WPAFB, OHIO

TABLE OF CONTENTS

GRAPHICS DISCLAIMER

All figures, graphics, tables, equations, etc. merged into this translation were extracted from the best quality copy available.

CONTROL OF SOLID-APOGEE MOTOR DURING ORBIT TRANSFER MANEUVER

Zhang Yuntong

(Beijing Institute of Spacecraft System Engineering)

Abstract

This paper provides a method for determining the optimum time and attitude in process of geostationary satellite launch at which the solid-apogee motor to be fired.

Subject Terms: firing time, satellite attitude, optimum design, Apogee engine

(The manuscript was received on July 13, 1989.)

I. Forward

In the process of launching geostationary satellites, the Apogee engine on the satellite provides an increment in the velocity of the satellite which, ultimately, transforms the orbit the satellite travels from a transitional orbit into a geostationary orbit. The direction of spin of a geostationary satellite is the direction of the velocity increment. Therefore, the orbit transition control of an Apogee engine is to determine the firing time and the spin direction (the so called firing attitude) for a given transitional orbit.

Different firing times and firing attitudes can result in different orbits after the engine is stopped. Hence, the firing time and firing attitude should be carefully chosen to obtain the optimum orbit. In

the actual engineering practices, the choice is always subjected to some limitations, and, therefore, this problem can be thought of as an constrained optimization problem. In this paper, we will introduce: (1) the working model of Apogee engines, (2) the definition of optimization target functions, and (3) method of optimization.

II. The Working Model of Apogee Engines

1. Equation of Motion

The equation of motion of the center-of-mass of a satellite during the working period of Apogee engine can be simplified as:

$$\left.\begin{aligned}\frac{d^2x}{dt^2} &= -\frac{\mu x}{r^3} + \frac{F}{m_0 - \dot{m}t}\cos\alpha\cos\beta \\ \frac{d^2y}{dt^2} &= -\frac{\mu y}{r^3} + \frac{F}{m_0 - \dot{m}t}\sin\alpha\cos\beta \\ \frac{d^2z}{dt^2} &= -\frac{\mu z}{r^3} + \frac{F}{m_0 - \dot{m}t}\sin\beta\end{aligned}\right\} \qquad (1)$$

where x, y, z are the coordinates of the satellite in the earth equatorial coordinate system; r is the distance from the satellite to earth's center; μ is earth's gravitational constant; F is the thrust of the Apogee engine; m_0 and $\dot{m}$ are the initial mass of the satellite and the rate of mass flow of propellent (per second); and α and β are the longitude and altitude of the firing attitude. The integration should be carried out in the time interval of the working period of the Apogee engine; namely, the integration starts at the time when the Apogee engine is ignited and stops when the Apogee engine is stopped.

After the transformed orbit is selected for a firing time t_0, the initial conditions for the set of equations (1) can be obtained and F, m_0, $\dot{m}$ and the working time of the Apogee engine are all fixed parameters. If a set of α and δ were chosen, the orbit of the satellite after the engine is stopped can be obtained from the integration of equation (1). In other words, for a set of firing time and firing attitude (t_0, α, δ), the orbit of the satellite after the engine is stopped can be calculated.

2. Pulsed Orbit-Transition Model

For solid-Apogee motors, the working time is on the order of a few tens of seconds. During its working period, the satellite is in the vicinity of the Apogee point. It can be assumed that the satellite obtains the velocity increment instantly. The position and velocity of the satellite at ignition and stop of the Apogee motor should be expressed in terms of the subscripts "0" and "f". Their relationship can be simplified as

$$\left.\begin{aligned} x_0 &= x_f \\ y_0 &= y_f \\ z_0 &= z_f \\ \dot{x}_0 &= \dot{x}_f + V\cos\alpha\cos\delta \\ \dot{y}_0 &= \dot{y}_f + V\cos\delta\sin\alpha \\ \dot{z}_0 &= \dot{z}_f + V\sin\delta \end{aligned}\right\} \qquad (2)$$

where V is the velocity increment provided by the Apogee motor and it quantity is:

$$V = g_0 I_{sp} \ln\frac{m_0}{m_0 - \dot{m}T}$$

where g_0 is the gravitational acceleration on the surface of the earth; I_{sp} is the specific impact in vacuum; and T is the working time of the motor. Similarly, if the firing time t_0 is determined, x_0, y_0,

z_0. $\dot{x}_0$. $\dot{y}_0$, $\dot{z}_0$ can be calculated from orbit measurement and α and δ are the quantities which should be chosen. The relationship between the parameters x_S, y_S, z_S, $\dot{x}_S$, $\dot{y}_S$, $\dot{z}_S$ and the orbital parameters is determined by the well known equations as those in [1].

3. Comparison and Conclusion of The Two Models

In the two methods mentioned above, method (1) is closer to the actual motion. When the working time of solid motors is a few tens of seconds, the difference of the calculated target functions can be ignored. The minimum difference in the target function is obtained when the difference in the firing times based on these two models is 0.55 times of the working time of the motor. Therefore, optimal condition can be obtained if the actual firing time is 0.55T in advance of the time based on the pulsed model.

III. Target Function

1. Definition of the Target Function

In order to evaluate the advantages and disadvantages of the chosen parameters t_0, α, and δ, the optimal target function is defined as: the corrective velocity increment necessary to bring the orbit at engine stop to the geostationary orbit. The optimum set of functional variables is the set of t_0, α, and δ which minimizes the target function.

2. Calculation of the Target Function

The orbital parameters at engine-stop are: geometrical longitude at engine-stop λ_1; half long-axis of the orbit a_1; orbital eccentric ratio e_s; orbital tilt angle j_s; equatorial longitude of the up-rising point Ω_1. The parameters of the geostationary orbit are: fixed position geometrical longitude λ_{w}; half long-axis of the orbit a_0; orbital tilt angle i_0; equatorial longitude of the up-rising point Ω_0. In order to maintain the north-south position, λ_{w} should be around 270° and i_0 should be about 0.1°. To maintain the east-west position, e_s should be less than a certain value and this value was taken as zero when the target function was calculated. The corrective velocity in the target function was expressed in terms of three parts:

(1) Corrective velocity ΔV_1 necessary for the correction of half long-axis and eccentric ratio:

To correct a_1, e_s to a_0,(e_0=0), a dual-pulse was required and the velocity was increased (or decreased) at the bunch point. The calculational equations are:

$$r_{1,1} = a_1(1-e_1)$$

$$V_{1,1}^2 = \mu\left(\frac{2}{r_{1,1}} - \frac{1}{a_1}\right)$$

$$V_1^2 = \mu\left(\frac{2}{r_{1,1}} - \frac{2}{a_1+a_0}\right)$$

$$V_2^2 = \mu\left(\frac{2}{a_0} - \frac{2}{a_1+a_0}\right)$$

$$V_2^2 = \mu\left(\frac{1}{a_0}\right)$$

The corrective velocity $\Delta V_1 = |V_{1,1} - V_1| + |V_2 - V_2|$

(2) Corrective velocity ΔV_2 necessary for fixed-point capture:

Assuming that $\lambda_1 > \lambda_w$, and in order to maintain the satellite at position λ_w, the satellite should drift towards the west after the

motor was stopped. If the rated drifting velocity is $\dot{\lambda}$ (degrees/day), $\dot{\lambda} < \dot{\upsilon}$. The half long-axis corresponding to the drift should be

$$a_d = \left(a_0 - \frac{\dot{\lambda}}{540^2} \cdot a_0\right)$$

The calculational equations for corrective velocity ΔV_1 according to various a_s and e_S are tabulated in table 1:

Table 1: Calculational equation for corrective velocities

表1 [illegible]

判别条件①			ΔV_1
$a_s > a_d$			0
$a_s < a_d$	$r_{ip} > a_0$		$\omega_Z (a_d - a_1)$
	$r_{ip} < a_0$	$a_1 > a_d$	0
		$a_s \leq a_1 \leq a_d$	$\omega_Z (a_0 - a_1)$
		$a_1 \leq a_s$	$\omega_Z (a_d - a_0)$

(key 1: condition)

In table 1, $\omega_z = \frac{V_1}{a_0}$ is the angular speed of earth's spin and

$$a_1 = \frac{1}{2}[a_0 + a_s(1 + e_s)]$$

(3) Corrective velocity ΔV_3 necessary for orbital plane capture:

Orbital plane capture is achieved by correcting i_s [illegible] to i_0 and Ω_s, and the orbital plane should be tilted an i_p angle,

$$\cos i_p = \cos i_s \cos i_0 + \sin i_s \sin i_0 \cos(\Omega_s - \Omega_0)$$

The corrective velocity can be approximated as:

when $i_p < \pi/2$, $\Delta V_3 = V_0 i_p$

when $i_p > \pi/2$, $\Delta V_3 = V_0(\pi - i_p)$ (i_p in radians)

If $\lambda_s < \lambda_0$, similar results can also be obtained.

3. Target Functional Values

The target function is $\Delta V = \Delta V_1 + \Delta V_2 + \Delta V_3$ and the relationship between the chosen parameters (t_0, α, δ) and the target function is explained in the above sections.

IV. Optimization Process

1. Method of Optimization

Under the normal conditions, in the process of satellite launching, the error encountered in the transition orbit is usually very small and the region for optimization is also a very narrow region; on the other hand, the calculation based on the pulsed model is also very simple. Based on these reasons, the method of optimization can be the reliable listing method and the searching can be carried out in the vicinity of the standard values.

2. Calculation of the Standard Values

It was assumed that the standard values satisfy the two conditions: 1) i_s, Ω_s equal i_0, Ω_0, respectively; 2) $\vec{r}_s$ and $\vec{V}_s$ are mutually perpendicular and $x_s\dot{x}_s+y_s\dot{y}_s+z_s\dot{z}_s=0$. Further, it was assumed that the instantaneous roots at the up-rising point before ignition of the motor were a_3, e_3, i_3, ω_3, Ω_3, M_3, replacing the instantaneous roots of at the ignition point. The calculation of the standard values of the firing time and firing attitude was then based on the familiar two-body equations:

$$\cos i_f = \cos i_0 \cos i_3 + \sin i_0 \sin i_3 \cos(\Omega_0 - \Omega_3)$$

$$\sin u_{30} = \sin(\Omega_3 - \Omega_0) \sin i_0 / \sin i_f$$

$$f_3 = u_{30} - \omega_3$$

$$E_3 = 2 \cdot \mathrm{tg}^{-1}\left[\sqrt{\frac{1-e_3}{1+e_3}}\mathrm{tg}\left(\frac{f_3}{2}\right)\right] \qquad \left(\frac{f_3}{2} \text{ 和 } \frac{E_3}{2} \text{ 同象限}\right) \text{①}$$

$$M = M_3 + E_3 - e_3 \sin E_3$$

$$\tilde{t} = M \Big/ \sqrt{\frac{\mu}{a_3^3}}$$

$$P_3 = a_3(1-e_3^2)$$

$$r_3 = P_3/(1+e_3\cos f_3)$$

$$V_3^2 = \mu\left(\frac{2}{r_3} - \frac{1}{a_3}\right)$$

$$\varepsilon_3 = \sin^{-1}[\sqrt{\mu P_3}/r_3 V_3] \quad (f_3 > \pi \text{ 时 } \varepsilon_3 \text{ 取第二象限}) \text{②}$$

$$\delta_3 = \sin^{-1}(\sin i_3 \sin(u_{30} + \varepsilon_3))$$

$$\alpha_3 = \Omega_3 + \mathrm{tg}^{-1}(\cos i_3 \mathrm{tg}(u_{30} + \varepsilon_3)) \qquad (\mathrm{tg}^{-1} \text{ 的象限与 } u_{30} + \varepsilon_3 \text{ 相同}) \text{③}$$

$$\cos\Psi_3 = \sin\varepsilon_3 \cos i_f$$

$$\cos x = -\mathrm{ctg}\varepsilon_3 \mathrm{ctg}\Psi_3$$

$$\sin\Psi_4 = \frac{V_3}{V_4}\sin\Psi_3$$

$$\cos\eta = -\mathrm{tg}\delta_3 \mathrm{ctg}(u_{30} + \varepsilon_3)$$

$$\sin\tilde{\delta} = \sin\delta_3 \cos(\Psi_3 + \Psi_4) + \cos\delta_3 \sin(\Psi_3 + \Psi_4)\cos(\eta + x)$$

$$\sin(\alpha_3 - \tilde{\alpha}) = \sin(\Psi_3 + \Psi_4)\sin(\eta + x)/\cos\tilde{\delta}$$

key - 1: $f_3/2$ and $E_3/2$ are in the **same** quadrant.

2: When f_3 is greater than π, ε_3 lies in the second quadrant.

3: tg^{-1} and $u_{30}+\varepsilon_3$ lie in the **same** quadrant.

3. Conclusion of the Optimization Process

The control of the orbit transfer maneuver of Apogee motor can be concluded as:

(1) measurement of the transition orbit:

(2) calculation of the standard values $\tilde{t}$, $\tilde{\alpha}$, $\tilde{\delta}$,

(3) confirmation of the region-of-choice and step-length of t, α and δ :

(4) calculation of the parameters a_s, e_s, i_s, Ω_s after stop of the motor for each set of t, α and δ ;

(5) calculation of the target function ΔV;

(6) repeat of steps (3) ~(5) to determine the t, α , and δ corresponding to the minimum ΔV;

(7) calculation of t-0.55T and (α, δ) for actual firing time and firing attitude, respectively.

REFERENCES

[1] J. W. Cornelisse, H. F. R. Schoyer, K. F. Wakker: "Rocket propulsion and Spaceflight Dynamics", p. 377

[2] Jiang, Jenwei: "Control of Orbit and Attitude of Geostationary Satellites", Science Publishing Corp., 1987

APPLICATION OF SPLIT-PHASE CODE PSK SIGNAL IN DATA TRANSMISSION OF METEOROLOGICAL SATELLITE REMOTE SENSING IMAGE

Dai Ying

(Shanghai Institute of Spacecraft Engineering)

Abstract

In this paper, split-phase code PSK signal is analyzed, its character is reviewed, the basic formation method is briefly described. The application of the signal in digital image transmission of astronautical remote sensing is introduced. And finally, photos of real-time data transmission are presented.

Subject Terms: phase shift keying, phase modulator, picture transmission, meteorological satellite, application

(The manuscript was received on May 5, 1989.)

(The definition of split-phase code can be found in reference 1.)

I. Split-Phase Code Phase-Shift Keying Signal

Split-phase code phase-shift keying (PSK) signal is the modulated signal of the carrier wave, based on the split-phase code signal, after phase-shift keying. It is a binary modulated signal; namely, the PCM-PSK/digital split-phase, which is also a primary phase-modulated signal without the auxiliary carrier waves. Its mathematical formula is:

$$S(t)=A_c\cos[\omega_c t+\Delta\varphi(t)] \qquad (1)$$

where u_m - amplitude;

ω_0 - frequency of the carrier wave;

$\Delta\varphi$ - split-phase code phase-shift amplitude, $\Delta\varphi = \frac{\pi}{2}$;

c(t) - split-phase code, its value should be taken as +1 or -1 randomly.

The relationship between the amplitude and phase-shift angle of the split-phase code PSK signal is:

$$\cos\Delta\varphi = \sqrt{\frac{2}{\pi}}\frac{u_{cm}}{u_m} \qquad (2)$$

where u_{cm} is the voltage amplitude of the modulated carrier wave.

In the process of product research and development, according to equation (2), the phase-shift amplitude of the carrier wave by the random split-phase code can be measured with the frequency spectroscope. Using this method, the modulation of the transmitter can be measured with higher accuracy. This equation can also be used in the orbital test of satellites.

The mathematical expression of the frequency spectrum of split-phase code PSK signal is:

$$F(\omega-\omega_c) = \pi\cos^2\Delta\varphi\frac{u_m^2}{2}\delta(\omega-\omega_0)$$

$$+\frac{T}{2}\sin^2\Delta\varphi\frac{u_m^2}{2}\left(\frac{\sin\frac{(\omega-\omega_0)T}{4}}{\frac{(\omega-\omega_0)T}{4}}\right)^2\cos^2\frac{(\omega-\omega_0)T}{4} \qquad (3)$$

where δ is a function with screening characteristics which is also called the δ function and T is the period of the split-phase code.

According to equation (3), the frequency spectrum can be plotted as shown in figure 1. The shape of coverage of the spectrum of this code

is similar to that of the fundamental band signal frequency spectrum of the split-phase code. Therefore, in order to avoid interference, it was only necessary to filter the visual wave, before modulation, to accomplish the intra-band constraint of the spectrum of split-phase code PSK signal. Technically, this method is easier to perform than the intra-band constraint of the microwave after modulation and, also, this method is more economically feasible.

The split-phase code PSK signal has certain characteristics which makes it very powerful in the digital image transmission. Firstly, since the phase shift angle of the split-phase code was not equal to $\pi/2$, the carrier wave part could be saved after modulation. Secondly, since the part of the fundamental frequency spectrum of the split-phase code at zero frequency was zero and the phase-shift modulation of the carrier wave was the linear transformation, the part of the carrier wave after modulation existed independently and the interference of the change of the message spectrum did not exist. This led to the features of stable carrier frequency part and the high signal to noise ratio. For example: when the narrow band in the vicinity of the carrier frequency in the frequency spectrum of the split-phase code $\Delta f=0.35\frac{1}{T}$时, the power of the message part of the continuous spectrum was less than 0.03% of the total power of the message spectrum and the actual signal to noise ratio could be as high as 75dB.

In figure 1, the percentages were the results of the numerical integration of equation (3) and indicated the power of each specific wave peak as compared to the total power of all the wave peaks in the continuous wave spectrum. One can see that most of the power of the

kev: 1 - carrier wave

2 - continuous frequency spectrum

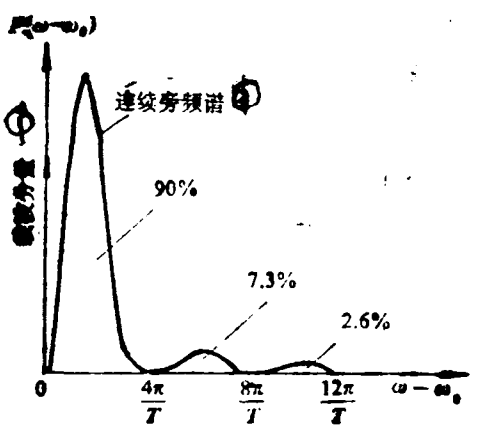

图 1 分相码移相键控信号频谱

Figure 1: Frequency spectrum of the split-phase code PSK signal

continuous wave spectrum existed in the first wave peak which amounted to 90%.

On the other hand, under the condition of total symmetry of the split-phase code, there was no dispersion frequencies of the modulated frequency spectrum of the split-phase code PSK signal. Also, there was no even parts. In this way, the erroneous tracking of the carrier wave by the ground station could be avoided.

With these special features, the split-phase code PSK signal was a useful tool in determining the modulation functions of a transmitter and the design of the match of system frequency band. If the band width which occupied 90% of the energy was 2.8MHz, considering 1) the frequency deviations caused by the carrier wave and the signal itself, 2) the acceptable signal to noise ratio and, 3) the deformation of the waveform of the signal, the band width of the receiver was chosen to be 3MHz. Even though the edge of this band width overlapped with the corresponding frequency spectrum of the TIROS-N satellite of USA, no interference should occur because of the separation in space and time.

If the special features of signal mentioned above were linked with the system function, the advantage of the split-phase code PSK signal was made even more obvious. For example, to transmit digital image with split-phase code PSK signal, when the receiving/demodulation equipment received the PSK signal, the PSK signal power which entered into the carrier wave lock-up phase loop of the receiver was very limited. In other words, even though the signal received was the modulated signal, the signal to noise ratio of the part of the carrier wave which entered into the loop was high. In this way, the signal could be transmitted under the condition without the modulation of

auxiliary carrier wave and the receiver could perform tracking of the carrier wave and de-modulation of the signal simultaneously.

The disadvantages of the split-phase code PSK signal was that when the signal was transmitted through wireless transmission, the interference would occur due to the effect of multi-path electrical transmission. Therefore, when the system was tested or measured, the geographic effect should be adequately taken into account.

II. The Formation of the Split-Phase Code PSK Signal

The split-phase code PSK signal was formed by keying the phase of the carrier wave signal with the split-phase code. In the following, two basic methods for the formation of split-phase code PSK signal would be briefly explained and mathematical methods were used to analyze the formation process.

Method 1:

The basic principle is shown in figure 2 and the relationship between various phases is shown in figure 3.

Figure 2 shows that the multiplier does not shift the phase of the carrier wave signal u(t) in the first half of the cycle of the split-phase code operation time, but in the second half of the operating cycle, u(t) is shifted 180 degrees. The mathematical analysis is: Let $u(t)=u_m\cos\omega_0 t$, when $0<t<\frac{T}{2}$ the output signal of the multiplier is

$$u_1(t)=ku_m\cos(\omega_0 t+\frac{\pi}{2})$$
$$=-u_{1m}\sin\omega_0 t$$

where k is a constant.

At the same time, the output signal of the adder is

key: 1 - phase shifter

2 - split-phase code signal

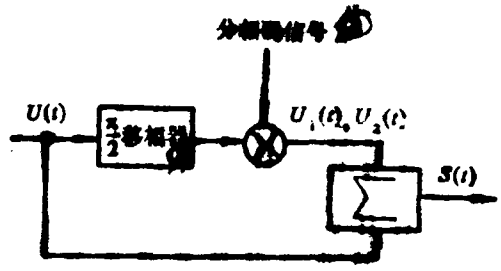

图 8

Figure 2: split-phase code phase shifting principle

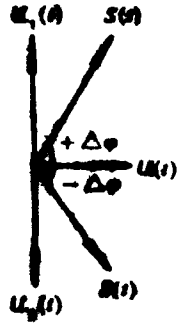

图 9

Figure 3: Phase relationship of various components

$$S(t) = u_m \cos\omega_0 t - u_{1m} \sin\omega_0 t$$
$$= A_m \cos(\omega_0 t + \Delta\varphi) \qquad (4)$$

where

$$A_m = \sqrt{u_m^2 + u_{1m}^2},$$
$$\Delta\varphi = \operatorname{arctg}\left|\frac{u_{1m}}{u_m}\right|.$$

Therefore, the phase-shifting modulation of the carrier wave by the positive electrical potential (subsidiary code "1") of the split-phase code was accomplished. When $\frac{T}{2} < \tau < T$, u(t) was shifted 180 degrees.

$$u_2(t) = ku_m \cos\left(\omega_0 t + \frac{\pi}{2} + \pi\right)$$
$$= u_{2m} \sin\omega_0 t$$
$$s(t) = u(t) + u_2(t)$$
$$= u_m \cos\omega_0 t + u_{2m} \sin\omega_0 t \qquad (5)$$
$$= A_m \cos(\omega_0 t - \Delta\varphi)$$

where $A_m = \sqrt{u_m^2 + u_{1m}^2}$,

$$-\Delta\varphi = \operatorname{arctg}\left|\frac{u_{1m}}{u_m}\right|.$$

Therefore, the phase-shifting modulation of the carrier wave by the negative electrical potential (subsidiary code "0") of the split-phase code was accomplished. It can also be seen that by controlling the accuracy in phase-shifting and the amplitude ratio of the two signals, the split-phase code PSK signal can be formed.

Method 2:

Figure 4 shows a reflective-type modulator which accomplishes the phase keying control of the carrier wave by controlling the path L of the carrier wave. When the split-phase code was at the positive electrical potential, the PIN tube was connected and point A was grounded and the carrier path was L_1. When the split-phase code was at

key: 1 - micro band matching network

2 - split-phase code

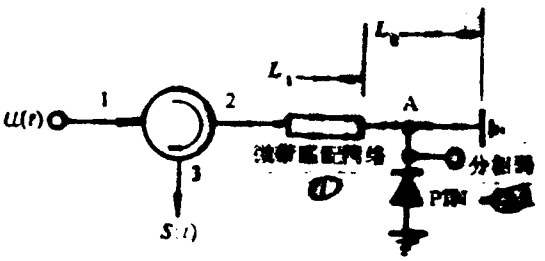

图4 一种反射型调相器

Figure 4: A reflective phase modulator

the negative electrical potential, the PIN tube was disconnected and the path of the carrier wave was L_2. If $\frac{2\pi}{\lambda}(L_2-L_1)=\Delta\varphi$ is satisfied, the carrier phase transformed from φ_1 to φ_2 can be obtained. φ_1 was the initial value.

In actual application, the 3dB bridge was used in replace of the cyclotron in figure 4. In fact, the modulator manufactured in this way would perform better and actual manufacturing was accomplished.

III. The Application of the Split-Phase Code PSK Signal

The split-phase code PSK signal was used not only in the digital communication of spacecraft, it was also used in the transmission of high resolution remote-sensing images of TIROS-N meteorological satellite. The meteorological satellites manufactured in China also used the split-phase code PSK signal to transmit ultra-high resolution cloud maps. This system consisted of two parts (satellite transmission and ground receiving):

Satellite Transmission: The satellite transmission included the electronic circuitries of the remote sensing system and the transmitter and antenna of the transmitting system. The remote-sensing system installed on the satellite was a five-channel scanning radiation monitor which received the thermal radiation data from the emission and reflection of the earth-atmosphere system and the visible light data which included the meteorological data from cloud top, earth surface and ocean.

The remote-sensing equipment first transformed the gathered data into electronic signals and then quantized and digitally processed

these signals. After coupling the service code, the information was edited and according to the special format requirement, such as the service code of synchronous signal, satellite attitude, earth meteorological data, and the error message detecting sequence, the binary code was transformed into the split-phase code. After phase-shifting keying of the carrier frequency of the transmitted cloud map data, the split-phase code PSK signal was generated. This signal was transmitted to ground, via antenna, after amplification.

Ground Receiving: After the ground station received the split-phase code PSK signal, the high-frequency part was amplified, the frequencies were mixed, intermediately amplified, and then transmitted to the lock-phase de-modulator. During de-modulation, the phase of the signal was compared with the phase of the split-phase code PSK signal carrier wave reference signal and the split-phase code signal was obtained. The amplified split-phase code was transmitted to the bit synchronizer to extract the synchronous clock signal and the split-phase code was transformed into the non-zero code and transmitted to the frame synchronizer. In the frame synchronizer, the beginning of a frame signal--the 60 bit pseudo-random signal was examined to extract the frame synchronous timing signal and the cloud maps or the earth meteorological signal was separated into five channels. For the error message signal at the end of a frame of signals, the error rate would be examined and rate of error message of the whole string of data would be derived. If the error rate satisfied the requirement, the cloud map signal would be transmitted to the data processing system for real-time image processing. Or, the data could be stored

for future processing to obtain the meteorological data of the cloud top, earth surface and ocean.

Figures 5 and 6 show two processed high resolution cloud maps which were transmitted by the high resolution cloud map transmission system (HRPT system) of the "Fong-Yun" No. 1 meteorological satellite via split-phase code PSK signal. Figure 5 shows the cloud map transmitted by the HRPT system at 08GMT on September 8, 1988. It shows the rain-producing cloud system of the south eastern part of China. In the southern part of China, there were several cloud strings which fed to the rain-producing cloud region. The dark region at the bottom of the figure was the South Sea and Hainan Island was at the center of it. Figure 6 shows the visible light high resolution meteorological cloud map transmitted by HRPT system, at the downstream of the Yangtze river at 6:30 GMT on September 20, 1988. This map shows clearly the cloud distribution and the sand content of the downstream of the Yangtze rive and the East Sea. It also shows the position of the five sand strips and the width of each string at the coastal region of the JiangSu province. Also, the south pointed dispersion of the fresh water from the Yangtze river in the ocean can be clearly seen. This dispersion of the fresh water affected the HangJu bay. Further, the mixing and distribution of the fresh water and sea water can be seen. (Figures 5 and 6 are in the third cover page.)

All of these figures have clear images and clear geographic boundaries. The resolution was less than 1km. One of the high resolution cloud maps was used by the "AVIATION WEEK" magazine.

Data transmission was one of the key issues to produce high quality cloud maps. Therefore, it should be noted that transmission of

the remote-sensing images by the split-phase code PSK signal was successful. These cloud maps provide important data for weather forecasting, typhoon monitoring, ocean detecting, and agricultural evaluation.

REFERENCES

[1] Yao, Yen et al.: "Digital Microwave Intermediate Communication", Peoples communication Publishing Corp., 1981. 6

[2] N76-31375, Integrated Source and Channel Encoded Digital Communication System Design Study

DISTRIBUTION LIST

DISTRIBUTION DIRECT TO RECIPIENT

ORGANIZATION	MICROFICHE
C509 BALLISTIC RES LAB	1
C510 R&T LABS/AVEADCOM	1
C513 ARRADCOM	1
C535 AVRADCOM/TSARCOM	1
C539 TRASANA	1
Q591 FSTC	4
Q619 MSIC REDSTONE	1
Q008 NTIC	1
E053 HQ USAF/INET	1
E404 AEDC/DOF	1
E408 AFWL	1
E410 AD/IND	1
F429 SD/IND	1
P005 DOE/ISA/DDI	1
P050 CIA/OCR/ADD/SD	2
AFIT/LDE	1
NOIC/OIC-9	1
CCV	1
MIA/PHS	1
LLYL/CODE L-309	1
[redacted]	1
NSA/T513/TDL	2
ASD/FTD/TTIA	1
FSL	1